

A VECTORIAL APPROACH TO COMPUTATIONAL MODELLING OF BEAMS UNDERGOING FINITE ROTATIONS

JAEWOOK RHIM[†] AND SUNG W. LEE^{*,‡}

Department of Aerospace Engineering, University of Maryland, College Park, MD 20742, U.S.A.

ABSTRACT

The description of finite rotations of beam-like structures using rotational parameters is not the most efficient, from a computational standpoint, because of the non-vectorial nature of finite rotations in three-dimensional space. In the present study, the classical rigid cross-section assumption is abandoned and the motions of beam directors in three-dimensional space is represented using vector quantities so that the resulting configuration space of a beam becomes a linear vector space. Issues concerning the proper constitutive relations are also discussed. Numerical results illustrate that the present approach produces attractive properties for various non-linear problems involving very large rotations compared to the conventional rotational parameter approach. © 1998 John Wiley & Sons, Ltd.

Int. J. Numer. Meth. Engng., **41**, 527–540 (1998)

KEY WORDS: vectorial kinematics; finite rotation; beam finite element

1. INTRODUCTION

1.1. General remarks

The interest in efficient and reliable modelling of beam-like structures is demonstrated by the significant body of literature devoted to this subject. Many structural members can be modelled as beams and their applications span a broad range of engineering fields. Especially, the computer-based geometrically non-linear analysis of flexible three-dimensional structures has attracted considerable interest in recent years. In the aerospace field, this is due to the establishment of challenging goals for space research, such as the space station, space-based antennae and telescopes, solar arrays and a variety of similar devices. Further interest comes from the need for efficient computational tools in stability analyses of weight-optimized, highly flexible frame structures, crash analyses and simulations of multi-body and free-flying body dynamics that exhibit pronounced geometrical non-linearities.

A general three-dimensional non-linear formulation is not a simple extension of a two-dimensional formulation because fully three-dimensional finite rotations have to be accounted for

* Correspondence to: S. W. Lee, Department of Aerospace Engineering, University of Maryland, College Park, MD 20742, U.S.A.

[†] Graduate Student, currently at Agency for Defense Development, Korea

[‡] Professor

that are not vector quantities.¹ This is in contrast with shell elements in which the nodal rotations are two-dimensional objects due to the absence of the drilling rotation.²

The use of rotation group (or orthogonal rotation tensor) in the kinematics of deformation is inevitable if the beam finite element formulation is to be constructed based on the classical rigid cross-section assumption. Among others, three-parameter representation of the rotation group such as the Euler angles and the rotation vector appears to lead the development of finite rotation beam elements due to its close link to the traditional concept of rotation and moment.^{3–14}

All formulations using rotational parameters suffer from one inherent drawback: they are restricted to small rotations between two successive load increments during the deformation process. This limitation arises because the configuration space of a beam is a non-linear function of rotational parameters and thus forming the incremental equilibrium equations for non-linear analyses requires the linearization of the configuration space. The formulations based on the approximation require small rotation increments and, consequently, small load increments leading to slow convergence.^{4,15} Other difficulties associated with the non-vectorial nature of three-dimensional finite rotations are the extra storage and calculations necessary to avoid the singularity and the unsymmetric tangent stiffness matrices resulting from the Eulerian treatment of the three-dimensional rotation.^{5,6} In dynamic analyses, the resulting mass and gyroscopic matrices are configuration-dependent, which increases the computational cost.^{6,7}

1.2. Historical review

Papers by Besseling^{16,17} appear to be the first ones in which the geometrical stiffness matrices for large deflections were established with the attention to the intricacies of rotational parameters. Argyris *et al.*^{18,19} developed an ingenious formulation entirely based on the concept of semi-tangential rotation which corresponds to the semi-tangential moments introduced by Ziegler.²⁰ Although the resulting tangent stiffness matrices are symmetric due to the semi-tangential rotation being commutative, the classical meaning of rotation and moment were lost and the formulation was restricted to straight beams.

A paper by Argyris³ triggered the virtually exclusive use of rotation vectors in the subsequent works on finite rotation analyses. Simo and Vu-Quoc⁵ proposed an Eulerian formulation adopting the classical concept of rotation. Thus, rotations were regarded as actions of the orthogonal group in the Euclidean 3-space which do not commute. The resulting tangent stiffness matrices are unsymmetric even for conservative loadings. They provided a configuration update procedure which is an algorithmic counterpart of the exponential map of a skew-symmetric matrix associated with the rotation vector, in which extra storage and manipulation for four quaternion parameters are necessary. Cardona and Geradin,⁶ using the rotation vector, gave general treatments of Eulerian, total and updated Lagrangian formulations. The use of Lagrangian formulation yielded symmetric tangent stiffness matrices. To avoid singularity in finite rotation analyses, frequent configuration updates are needed and the rotational vector should be corrected in a global sense. Ibrahimbegovic *et al.*⁸ also followed this approach. In these papers, the linearization of the equilibrium equations were achieved with the aid of the concept of directional derivative in the theory of non-linear manifolds.²¹

There are numerous papers in which authors used linearizations different from that of the papers mentioned above. Surana and Sorem⁴ and Dvorkin *et al.*⁹ employed the degenerated beam concept to develop total Lagrangian formulations. Euler angles⁴ and a rotation vector⁹ were chosen as kinematic variables and the quadratic terms in the series expansion of rotation tensor were kept in

the linearization process. Kouhia²² and Saleeb *et al.*²³ pointed out the importance of including the quadratic terms in their rotational parameter formulation for buckling analysis. A beam model based on a helicoidal approximation was proposed by Borri and Bottasso.²⁴ Danielson and Hodges²⁵ used the method of a decomposition of the rotation tensor.

The co-rotational approach seems to offer a non-linear framework in which standard linear formulations are used with respect to the rotating frame and non-linearity is introduced via the rotation of this frame. Earlier works on the co-rotational approach^{26,27} simply apply transformation matrices to linear stiffness matrices not accounting for the variation of these transformation matrices. Bathe and Bolourchi¹⁰ developed a three-dimensional degenerated beam element based on Euler angles. Rotation vector based co-rotational elements can be found in References 11 and 12. A notable contribution to the co-rotation formulation was made by Rankin and Nour-Omid,²⁸ who developed an element-independent algorithm where the invariance principle of rigid-body rotation is satisfied. Because the geometrical non-linearity comes only from the rigid-body rotation, these formulations are restricted to small strain problems. A recent article by Atluri and Cazzani²⁹ provides a comprehensive exposition including an extensive list of references on finite rotations in computational solid mechanics.

1.3. Objectives, scope and outline

The existing finite elements for finite rotation beams suffer from limitations associated with the use of rotational parameters. To overcome these limitations, a completely different approach is taken in this study. In the present kinematics of deformation, the traditional rigid cross-section assumption in bending is discarded and the cross-sections are allowed to deform in their own planes. The result of this choice is that in contrast with the rotational parameter approach, the configuration space of the beam becomes a linear vector space in which the exact linearization exists and the configuration update can be achieved by simple vector additions. The cross-sectional warping is also considered because the warping can significantly affect the response and stability of structures.^{30,31}

The first objective of this paper is to derive a consistent finite element formulation based on the classical director approach and the vectorial description of the director displacement field. Due to the three-dimensional nature of the resulting strain field, a proper beam constitutive law needs to be considered. The second objective is to demonstrate through numerical tests that the proposed formulation possesses computational advantages over the rotational parameter approach in non-linear response and stability analyses owing to the vectorial kinematics.

2. GEOMETRY AND KINEMATICS OF DEFORMATION

In the following, Latin indices have the values 1, 2 and 3, Greek indices 1 and 2, and repeated indices in a term are summed over the appropriate values.

Consider a three-dimensional slender beam in Figure 1. For the description of geometry and kinematics of deformation, a fixed global Cartesian co-ordinate system (x, y, z) is defined with unit vectors \mathbf{e}_i . Let a curve \mathcal{C} , the *beam axis*, embedded in three-dimensional space \mathbb{R}^3 , be defined by the equation

$$\mathbf{x}_0 = \mathbf{x}_0(\beta_3) \quad (1)$$

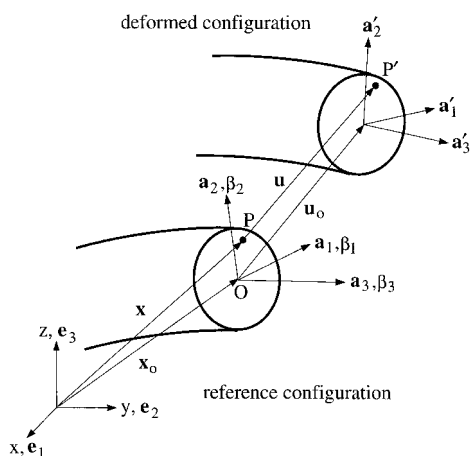


Figure 1. Geometry and kinematics of deformation

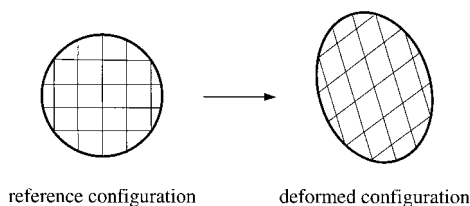


Figure 2. Graphical interpretation of the uniformly deformable cross-section

where \mathbf{x}_0 is the position vector of a point on \mathcal{C} in the initial undeformed configuration. β_3 is regarded as a convected co-ordinate defining points on the curve \mathcal{C} . Let

$$\mathbf{a}_3 \triangleq \frac{\partial \mathbf{x}_0}{\partial \beta_3} \tag{2}$$

be a unit vector tangent to the curve. Without loss of generality, β_3 can always be chosen so that $\|\mathbf{a}_3\| = 1$. A beam is defined to be a curve at each point of which there are two assigned *directors*. Thus, two directors \mathbf{a}_α which are orthonormal in the reference (undeformed) configuration, are assigned to every point of \mathcal{C} . Let β_α be the material co-ordinates along \mathbf{a}_α . Then $(\beta_1, \beta_2, \beta_3)$ form a curvilinear co-ordinate system along the beam axis.

Let \mathbf{x} be the position vector of a generic point P in the cross-section normal to the beam axis at \mathbf{x}_0 . With the above definitions of the co-ordinate systems at hand, the position vector \mathbf{x} can be expressed in terms of the global co-ordinates as

$$\mathbf{x} = \mathbf{x}_0 + \beta_\alpha \mathbf{a}_\alpha \tag{3}$$

To parameterize the displacement field, the classical assumption of rigid cross-sections in bending is abandoned. That is, any initially straight line segment on a cross-section remains straight and the angle of distortion is constant over the cross-section after deformation. The geometrical

interpretation is depicted in Figure 2. As the body deforms, \mathbf{a}_α become \mathbf{a}'_α and the vector \mathbf{a}'_3 can be formed such that

$$\mathbf{a}'_3 = \mathbf{a}'_1 \times \mathbf{a}'_2 \tag{4}$$

is still normal to the deformed cross-section. The vectors \mathbf{a}'_1 and \mathbf{a}'_2 are allowed to change their lengths and the condition $\mathbf{a}'_1 \cdot \mathbf{a}'_2 = 0$ is no longer valid according to the present assumption of deformable cross-section. Therefore, the three-dimensional motions of the two directors can be completely described with six vector components.

Taking into account the cross-sectional warping, the displacement of a point \mathbf{u} can then be expressed as

$$\mathbf{u} = \mathbf{u}_0 + \beta_\alpha \mathbf{u}_\alpha + \mathbf{u}_f \tag{5}$$

where \mathbf{u}_0 is the translational displacement of the beam axis, the director displacement vectors \mathbf{u}_α are defined as

$$\mathbf{u}_\alpha \triangleq \mathbf{a}'_\alpha - \mathbf{a}_\alpha \tag{6}$$

and \mathbf{u}_f represents the cross-sectional warping displacement.

The warping of the cross-section is represented by a warping displacement field superimposed over the flat cross-section parallel to the beam axis in the deformed configuration. For this purpose, the vector \mathbf{A}_3 is defined such that it is in the direction of the beam axis in the deformed configuration:¹³

$$\mathbf{A}_3 = \frac{\partial(\mathbf{x}_0 + \mathbf{u}_0)}{\partial\beta_3} \tag{7}$$

Then the warping displacement \mathbf{u}_f can be written as

$$\mathbf{u}_f = b(\beta_3)W(\beta_1, \beta_2)\mathbf{A}_3 \tag{8}$$

where W is a suitably chosen warping function and b is its coefficient. The unit vector \mathbf{a}'_3 differs from \mathbf{A}_3 in direction because of the non-zero transverse shear strains.

In the absence of warping, the configuration space under the present approach is a linear vector space where the exact configuration update is achieved by simple vector addition. This is in contrast with the conventional rotational parameter approach based on the rigid cross-section assumption.

3. FINITE ELEMENT MODELLING

For a three-dimensional body in equilibrium state, the principle of virtual work states that

$$\int_V (\delta\mathbf{E})^T \mathbf{S} dV - \delta W = 0 \tag{9}$$

where \mathbf{S} is the second Piola–Kirchhoff stress vector, \mathbf{E} is the Green–Lagrange strain vector and δW is the external virtual work. The volume integration is carried out over the reference (undeformed) configuration. The Green–Lagrange strain vector \mathbf{E} is defined as

$$\mathbf{E} = (E_{11} \ E_{22} \ E_{33} \ 2E_{12} \ 2E_{23} \ 2E_{31})^T \tag{10}$$

where E_{ij} are the components of the Green–Lagrange strain tensor measured in the curvilinear co-ordinate system $(\beta_1, \beta_2, \beta_3)$.³² The second Piola–Kirchhoff stress vector is related to the strain vector such that

$$\mathbf{S} = \mathbf{C}\mathbf{E} \quad (11)$$

where \mathbf{C} is the linear elastic material stiffness matrix.

Based on equations (1) and (5) the strain vector \mathbf{E} can be symbolically approximated as

$$\mathbf{E} = \sum P_k \mathbf{E}_k \quad (12)$$

In the above equation, \mathbf{E}_k are dependent on β_3 only, while P_k is independent of β_3 . The first term in equation (9) can then be integrated *a priori* over the cross-sections. In the finite element modelling, the \mathbf{x}_0 and \mathbf{a}_x vectors describing geometry and kinematic variables \mathbf{u}_0 , \mathbf{u}_x and b are then expressed in terms of the nodal values with the nodes located along the β_3 -axis.

Unlike conventional beam theories based on the rigid cross-section assumption, the extensional strains (E_{11} and E_{22}) and the in-plane shear strain (E_{12}) have non-zero values under the present kinematic assumption. Therefore, a three-dimensional constitutive relation involving six components of strain and stress must be established. However, the use of the classical Hookean law yields grossly erroneous results because the coupling between axial strains and axial stresses causes the deformed states to violate the assumption in the kinematics of deformable cross-section.¹⁵ A stress–strain relationship which is consistent with the kinematics of deformation is constructed by first expressing strain in terms of stress such that

$$\mathbf{E} = \bar{\mathbf{C}}\mathbf{S} \quad (13)$$

where $\bar{\mathbf{C}}$ is the 6×6 matrix of elastic compliance coefficients of a given material. The off-diagonal terms are set to zero and the resulting matrix is then inverted to obtain the desired \mathbf{C} matrix. For orthotropic materials, this process leads to a material stiffness matrix expressed as follows:

$$\mathbf{C} = \begin{pmatrix} E_1 & 0 & 0 & 0 & 0 & 0 \\ 0 & E_2 & 0 & 0 & 0 & 0 \\ 0 & 0 & E_3 & 0 & 0 & 0 \\ 0 & 0 & 0 & G_{12} & 0 & 0 \\ 0 & 0 & 0 & 0 & G_{23} & 0 \\ 0 & 0 & 0 & 0 & 0 & G_{31} \end{pmatrix} \quad (14)$$

where E_i and G_{ij} are the Young's moduli and the shear moduli, respectively. For isotropic materials, single values of Young's modulus E and shear modulus G are used.

Among the six components of strain, the magnitude of the axial strain E_{33} is much larger than those of the other strain components. For thin beams undergoing bending actions, the condition that all strain components except E_{33} become zero induces the element locking because E_{33} and the other strain components are kinematically coupled. The locking can be eliminated by the reduced numerical integration relaxing the zero strain condition as long as the reduced integration does not trigger any spurious kinematic modes.

Table I. Deflections of a pinched ring—locking test

Number of elements	Normalized deflection w		
	$R/t = 10$	$R/t = 100$	$R/t = 1000$
2	0.981	0.956	0.955
4	1.014	0.995	0.994
8	1.009	0.999	0.999
16	1.008	1.000	1.000

4. NUMERICAL TESTS AND DISCUSSIONS

Several non-linear benchmark tests are conducted to demonstrate that the proposed vectorial kinematics of deformation produces improved incremental/iterative performances over the rotational parameter approach. Three node quadratic elements with nine degrees of freedom per node are used in the numerical tests. The reduced integration (the two-point Gaussian quadrature in this case) is employed to eliminate the element locking.

A full Newton–Raphson solution procedure under the total Lagrangian setting is employed in all the calculations reported herein. Convergence of the finite element solution is established based on the Euclidean norm of the normalized incremental displacement. The criteria is

$$\frac{1}{2} \left(\frac{\|\Delta \mathbf{q}_t\|}{\|^{(n)} \mathbf{q}_t\|} + \frac{\|\Delta \mathbf{q}_d\|}{\|^{(n)} \mathbf{q}_d\|} \right) < \varepsilon_s \quad (15)$$

where $\Delta \mathbf{q}$ is the incremental displacement vector and $^{(n)} \mathbf{q}$ is the accumulated displacement vector at the current state and ε_s is an error tolerance. A value of $\varepsilon_s = 10^{-4}$ is used for all of the calculations. The subscripts d and t denote the nodal degrees of freedom corresponding to \mathbf{u}_x and to \mathbf{u}_0 and b in equations (5) and (8).

To trace the non-linear equilibrium paths, a modified arc-length method³³ is employed and the instability points are sought through criteria suggested by Bergan³⁴ in which the determinant of the tangent stiffness matrix and the stiffness parameter play key roles.

Simple polynomial functions are used as the basis of warping function $W(\beta_1, \beta_2)$ in this study. For example, skew-symmetric polynomials such as $\beta_1 \beta_2$, $\beta_1^3 \beta_2$ and $\beta_1 \beta_2^3$ produce excellent results for rectangular cross-sections.

4.1. Pinched ring—locking test

A circular ring of unit width subject to two opposite concentrated loads as shown in Figure 3 is chosen to test the effects of the locking as the radius-to-thickness ratio becomes very large. Owing to the symmetry of geometry and loading condition, only a quarter of the ring is modelled with the proposed elements. An isotropic material with Young's modulus of $E = 10^7$ psi and shear modulus of $G = 5 \times 10^6$ psi is used.

Three meshes of 2, 4, 8 and 16 elements equally spaced along the circumference and three values of radius-to-thickness ratio R/t are used to parameterize the curvature effect. Linear analyses is conducted with unit loading $P = 1$ lb to calculate the deflections of the loading points w . Table I lists the deflections of the loading points normalized by the theoretical value.³⁵ Calculated and theoretical values are in excellent agreement as convergence is achieved with eight elements.

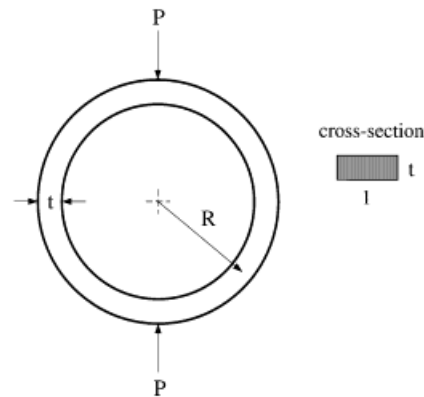


Figure 3. Circular ring under concentrated loads

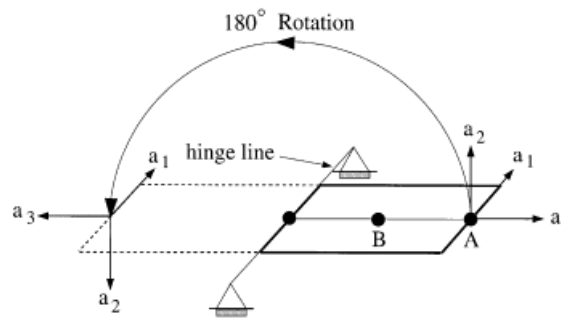


Figure 4. 180° rigid-body rotation of a single element

These results demonstrate that the proposed element, having six non-zero strain components, is very accurate and free of locking under the reduced integration.

4.2. Rigid-body rotation test

Because the strain energy and the internal stress of a deformable body should be invariant under any amount of rigid-body rotations, passing a rigid-body rotation test is one of the crucial requirements for finite elements to simulate deformations involving finite rotations accurately. For this reason, a 180° rigid-body rotation of a hinged beam modelled with one element as shown in Figure 4 is considered. The beam is 10 in long, 0.3 in thick, and with unit width. An isotropic material with Young's modulus of $E = 10^6$ psi and shear modulus of $G = 4 \times 10^5$ psi is used. A displacement control is applied in one step.

Table II contains the convergence behaviour of the axial stress S_{33} and shear stress S_{23} at the centre of the beam and the normalized error ε defined in equation (15). Surprisingly, convergence is achieved with only one non-linear iteration following a linear analysis. The invariance condition, i.e. the zero stress condition of rigid-body rotation is also verified. These results illustrate the importance of the exact linearization and configuration updating guaranteed by the present vectorial description of the director displacement field.

Table II. Convergence behaviour of the 180° rigid-body rotation

	Linear analysis	Non-linear iterations		
		1	2	3
S_{33}	0.2841×10^5	0.3433×10^{-7}	0.1787×10^{-9}	0.3062×10^{-9}
S_{23}	0.1943×10^4	0.7783×10^{-9}	0.2566×10^{-10}	0.8003×10^{-10}
ϵ	1.000	0.7073×10^{-5}	0.3551×10^{-8}	0.1950×10^{-9}

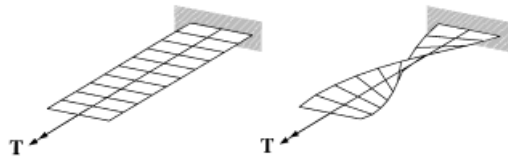


Figure 5. 180° twist of a cantilever beam

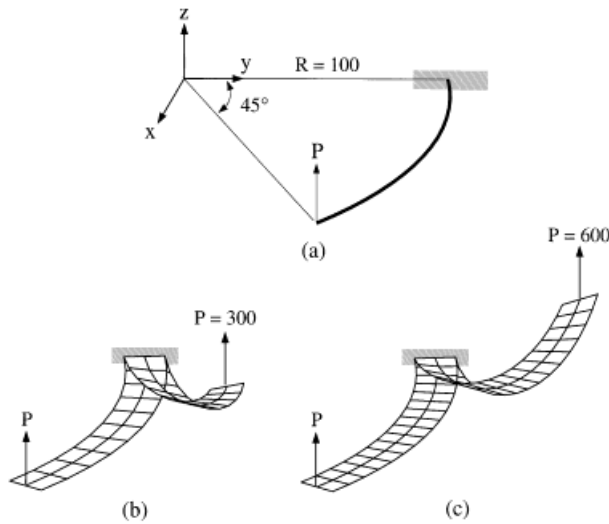


Figure 6. (a) 45° bending problem; (b) deformed shapes for $P = 300$ lb and (c) $P = 600$ lb

4.3. 180° twist of a cantilever beam

A cantilever beam subject to an end torque T is considered to examine torsional behaviour of the proposed element. The beam is 10 in long, 0.25 in wide, and 0.1 in thick. An isotropic material with Young's modulus of $E = 12 \times 10^6$ psi and shear modulus of $G = 4.6 \times 10^6$ psi is used. The beam is modelled with five elements. Because no angles are used in the present finite element formulation, torques are modelled as forces following the motion of directors.

The convergence is achieved in 15 Newton–Raphson iterations. The midplane of the undeformed and deformed configurations are shown in Figure 5. The total load needed to reach the 180° twist is approximately 7760.3 in lb, applied in only one load step. No previous solution of this problem

Table III. Tip displacements of a 45° bend

Element	Tip displacement (u, v, w)	
	$P = 300$ lb	$P = 600$ lb
<i>Present</i>	(-7.13, -12.03, 40.31)	(-13.70, -23.64, 53.46)
Bathe and Bolourchi ¹⁰	(-6.8, -11.5, 39.5)	(-13.4, -23.5, 53.4)
Crisfield ¹¹	(-7.13, -12.18, 40.53)	(-13.69, -23.87, 53.71)
Simo and Vu-Quoc ⁵	(-6.96, -11.87, 40.08)	(-13.50, -23.48, 53.37)
Cardona and Geradin ⁶	(-7.15, -12.07, 40.35)	(-13.74, -23.67, 53.50)
Dvorkin <i>et al.</i> ⁹	Not reported	(-13.6, -23.5, 53.3)
Surana and Sorem ⁴	Not reported	(-13.3, -23.7, 53.2)

Table IV. Incremental/iterative performance for the 45° bend—Comparison

Element	$P = 300$ lb		$P = 600$ lb	
	Load steps	Iterations	Load steps	Iterations
<i>Present</i>	1	8	1	13
Bathe and Bolourchi ¹⁰		60 equal increments		
Crisfield ¹¹	1	9	3	17
Simo and Vu-Quoc ⁵	1	13	3	27
Cardona and Geradin ⁶		6 equal increments, total 47 iterations		
Dvorkin <i>et al.</i> ⁹		10 equal increments, total 34 iterations		
Surana and Sorem ⁴		10 equal increments, total 35 iterations		

using a beam element has been reported. Only recently, Simo *et al.*³⁶ conducted this test using a shell element using rotation vectors as kinematic variables. They reported that they had a converged result, but did not state what the total load was or the number of iterations required. Three load steps were needed in their calculation.

4.4. 45° bend subject to an out-of-plane force

A 45° bend of unit square cross-section and radius of 100 in subject to an out-of-plane shear load P as shown in Figure 6(a) is modelled with 5 and 8 elements for $P = 300$ lb and $P = 600$ lb, respectively. An isotropic material with Young's modulus of $E = 10^7$ psi and shear modulus of $G = 5 \times 10^6$ psi is used for this problem. This example involves a genuinely three-dimensional response and has been studied by a number of authors using the rotational parameter approach.

The undeformed and deformed configurations are shown in Figures 6(b) and 6(c). Table III compares the present solution with those given by a number of authors for the tip displacements. Table IV compares the incremental/iterative performances. This type of comparison cannot be definite because of different convergence criteria but does give an overall trend. The converged solutions of numerous elements including the present one are so close to one another that no practical distinction can be made in terms of accuracy. However, the incremental/iterative performance of the proposed element is far better than existing ones. Only the proposed element converges for

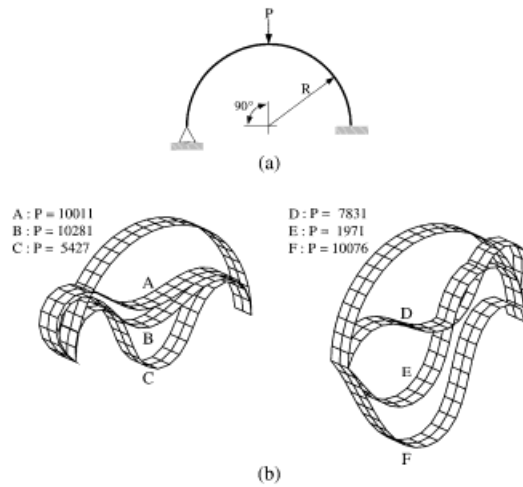


Figure 7. (a) Clamped-hinged deep circular arch subject to a concentrated downward force at the apex. (b) Deformed shapes of the clamped-hinged circular arch for various load levels

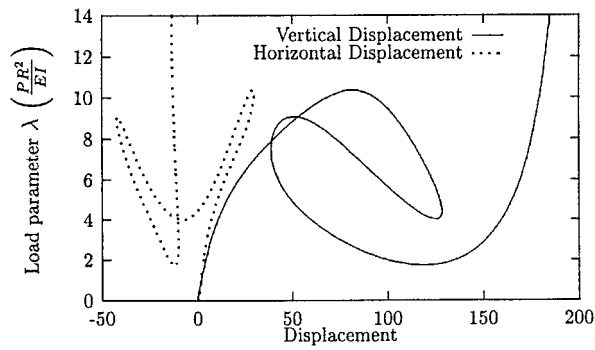


Figure 8. Equilibrium path of the clamped-hinged deep circular arch

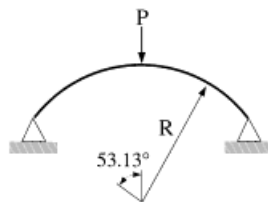


Figure 9. Hinged deep circular arch subject to a concentrated downward force at the apex

$P = 600$ lb in one load step and the number of iterations required is significantly less than the other elements listed in Table IV. These results demonstrate that the present vectorial description of the director displacement field is more effective than the rotational parameter description, especially in the problems involving three-dimensional large rotations.

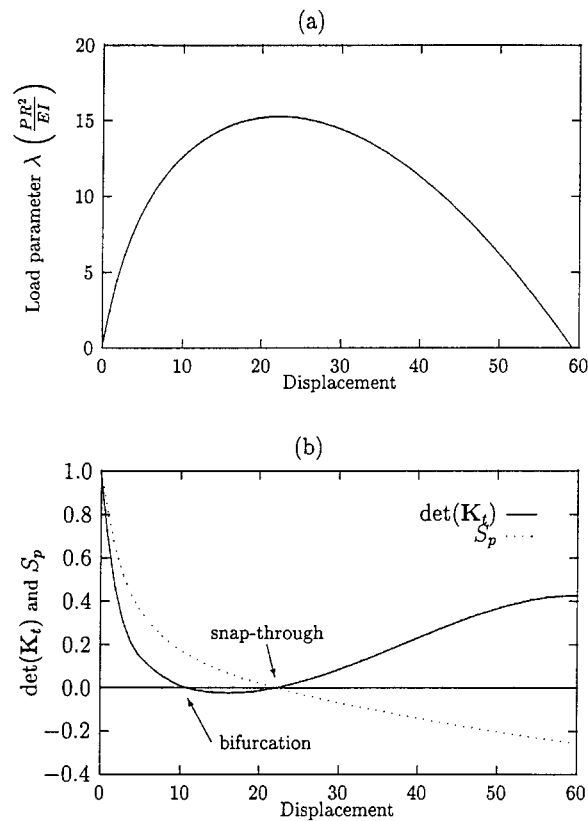


Figure 10. Non-linear behaviour of the clamped-hinged deep circular arch: (a) load-deflection curve; (b) stiffness parameter S_p and determinant $\det(\mathbf{K}_t)$

4.5. Buckling of a clamped-hinged circular arch

Consider a clamped-hinged circular arch as shown in Figure 7(a) subjected to a downward point load P at the apex. The radius R is 100 units and the cross-section is a unit square. An isotropic material with Young's modulus of $E = 12 \times 10^7$ and shear modulus of $G = 6 \times 10^7$ is used. This arch undergoes limit point bucklings due to its unsymmetry of the boundary condition. The entire arch is discretized with 12 equally spaced curved elements.

The deformed configurations for various values of load levels are shown in Figure 7(b) illustrating how the structure gradually becomes unstable undergoing large rotations. The entire non-linear equilibrium path is shown in Figure 8. The postbuckling behaviour of this particular structure is very unusual—four limit points and a pair of turning points. The analytical solution for the critical load (the first limit point load) based on the Kirchhoff–Love theory given by DaDeppo and Schmidt³⁷ is $P = 10270$ and in agreement with the calculated value of $P = 10310$.

4.6. Hinged deep arch under an apex load

A hinged circular arch subject to a central point load P is shown in Figure 9. The radius R is 100 units and the cross-section is a unit square. An isotropic material with Young's modulus

$E = 10^6$ and shear modulus $G = 3.8 \times 10^5$ is used. This structure has two instability points on the non-linear path with bifurcation occurring before the limit point is reached. The entire arch is modelled with 10 equally spaced curved elements.

The non-linear equilibrium path, shown in Figure 10(a), is traced until the applied force P vanishes after the snap-through of the arch. The stiffness parameter S_p^{34} and the determinant of tangent stiffness matrix $\det(\mathbf{K}_t)$ are calculated at every iteration to detect the instabilities as shown in Figure 10(b). The calculated bifurcation and limit points are $P = 13.0EI/R^2$ and $P = 15.2EI/R^2$, respectively. These values are identical to Huddleston's analytic solution.³⁸

5. CONCLUSIONS

A finite element formulation for analysis of finite rotation beam problems has been developed. Whereas existing finite element formulations for finite rotation problems are solely based on the rigid cross-section assumption and thus various types of rotational parameters are inevitably used as kinematic variables, the present formulation abandons the classical rigid cross-section assumption so that the three-dimensional evolution of directors can be represented by displacement vectors. Accordingly, in the absence of cross-sectional warping, the configuration space becomes a linear vector space where the exact configuration updating and linearization can be achieved regardless of the size of displacement increments.

The proposed vectorial approach improves the overall performance of beam finite elements in various non-linear response analyses. For the example problems tested in the present paper, single-load-step convergence is achieved with significantly fewer number of iterations than the rotational parameter finite elements require, regardless of the magnitude of rotations. Non-linear equilibrium paths including limit point and bifurcation instabilities are accurately traced using a simple continuation method.

Based on the observations made in this study, the vectorial approach can be applied to the areas where the finite rotation and stability considerations make the computation costly, such as collapse and crash analyses. Further development of the beam finite elements using the vectorial approach for multi-body and free-flying-body dynamics appears promising because of the improved performance on large (rigid-body) rotations and the configuration independent mass matrix which could render the dynamic simulations significantly efficient.

REFERENCES

1. J. Stuelpnagel, 'On the parametrization of the three-dimensional rotation group', *SIAM Rev.*, **6**(4), 422–430 (1964).
2. C. Sansour and H. Bufler, 'An exact finite rotation shell theory, its mixed variational formulation and its finite element implementation', *Int. J. Numer. Meth. Engng.*, **34**, 73–115 (1992).
3. J. H. Argyris, 'An excursion into large rotations', *Comput. Methods Appl. Mech. Engng.*, **32**, 85–155 (1982).
4. K. S. Surana and R. M. Sorem, 'Geometrically non-linear formulation for three-dimensional curved beam elements with large rotations', *Int. J. Numer. Meth. Engng.*, **28**, 43–74 (1989).
5. J. C. Simo and L. Vu-Quoc, 'A three-dimensional finite-strain rod model. Part II: computational aspects', *Comput. Methods Appl. Mech. Engng.*, **58**, 79–116 (1986).
6. A. Cardona and M. Geradin, 'A beam finite element non-linear theory with finite rotations', *Int. J. Numer. Meth. Engng.*, **26**, 2403–2438 (1988).
7. J. C. Simo and L. Vu-Quoc, 'On the dynamics in space of rods undergoing large motions—a geometrically exact approach', *Comput. Methods Appl. Mech. Engng.*, **66**, 125–161 (1988).
8. A. Ibrahimbegovic, F. Frey and I. Kozar, 'Computational aspects of vector-like parametrization of three-dimensional finite rotations', *Int. J. Numer. Meth. Engng.*, **38**, 3654–3673 (1995).
9. E. N. Dvorkin, E. Onate and J. Oliver, 'On a non-linear formulation for curved Timoshenko beam elements considering large displacement/rotation increments', *Int. J. Numer. Meth. Engng.*, **26**, 1597–1613 (1988).

10. K. J. Bathe and S. Bolourchi, 'Large displacement analysis of three-dimensional beam structures', *Int. J. Numer. Meth. Engng.*, **14**, 961–986 (1979).
11. M. A. Crisfield, 'A consistent co-rotational formulation for non-linear, three-dimensional, beam-elements', *Comput. Methods Appl. Mech. Engng.*, **81**, 131–150 (1990).
12. J. S. Sandhu, K. A. Stevens and G. A. O. Davis, 'A 3-D, co-rotational, curved and twisted beam elements', *Comput. Struct.*, **35**, 69–79 (1990).
13. A. D. Stemple and S. W. Lee, 'A finite element model for composite beams undergoing large deflection with arbitrary cross-sectional warping', *Int. J. Numer. Meth. Engng.*, **28**, 2143–2160 (1989).
14. M. Iura and S. N. Atluri, 'On a consistent theory, variational formulation of finitely stretched and rotated 3-D space-curved beams', *Comput. Mech.*, **4**, 73–88 (1989).
15. J. Rhim, 'A vectorial approach to finite rotation beams', *Ph.D. Dissertation*, University of Maryland at College Park, College Park, MD, August 1996.
16. J. F. Besseling, 'A nonlinear analysis of structures by the finite element method as a supplement to a linear analysis', *Comput. Methods Appl. Mech. Engng.*, **3**, 173–194 (1974).
17. J. F. Besseling, 'Derivations of deformation parameters for bar elements and their use in buckling and post-buckling analysis', *Comput. Methods Appl. Mech. Engng.*, **12**, 92–124 (1977).
18. J. H. Argyris, P. C. Dunne, G. Malejannakis and D. W. Scharpf, 'On large displacement—small strain analysis of structures with rotational degree of freedom', *Comput. Methods Appl. Mech. Engng.*, **14**, 401–451 (1978).
19. J. H. Argyris, O. Hilbert, G. A. Malejannakis and D. W. Scharpf, 'On the geometric stiffness of a beam in space—a consistent v. w. approach', *Comput. Methods Appl. Mech. Engng.*, **20**, 105–131 (1979).
20. H. Ziegler, *Principles of Structural Stability*, 2nd edn, Birkhauser, Basel, 1977.
21. J. E. Marsden and T. J. R. Hughes, *Mathematical Foundations of Elasticity*, Prentice-Hall, Englewood Cliffs, N.J., 1983.
22. R. Kouhia, 'On kinematical relations of spatial framed structures', *Comput. Struct.*, **40**(5), 1185–1191 (1991).
23. A. F. Saleeb, T. Y. P. Chang and A. S. Gendy, 'Effective modelling of spatial buckling of beam assemblages, accounting for warping constraints and rotation-dependency of moments', *Int. J. Numer. Meth. Engng.*, **33**, 469–502 (1992).
24. M. Borri and C. Bottasso, 'An intrinsic beam model based on a helicoidal approximation—Part I: formulation', *Int. J. Numer. Meth. Engng.*, **37**, 2267–2289 (1994).
25. D. A. Danielson and D. H. Hodges, 'Nonlinear beam kinematics by decomposition of the rotation tensor', *J. Appl. Mech.*, **54**, 179–184 (1987).
26. K. M. Hsiao, H. J. Horng and Y. R. Chen, 'A corotational procedure that handles large rotations of spatial beam structures', *Comput. Struct.*, **27**(6), 769–781 (1987).
27. C. C. Rankin and F. A. Brogan, 'An element independent corotational procedure for treatment of large rotations', in L. H. Sobel and K. Thomas (eds.), *Collapse Analysis of Structures*, ASME, New York, 1984, pp. 85–100.
28. C. C. Rankin and B. Nour-Omid, 'The use of projectors to improve finite element performance', *Comput. Struct.*, **30**, 257–267 (1988).
29. S. N. Atluri and A. Cazzani, 'Rotations in computational solid mechanics', *Arch. Comput. Methods Engng. State Art Rev.*, **1**(1), 49–138 (1995).
30. V. Z. Vlasov, *Thin-walled Elastic Beams*, 2nd edn, Israel Program for Scientific Translation, Jerusalem, Israel, 1961.
31. E. Reissner, 'On a variational analysis of finite deformations of a prismatical beams and on the effect of warping stiffness on bucking loads', *J. Appl. Math. Phys.*, **35**, 247–251 (1984).
32. A. E. Green and W. Zerna, *Theoretical Elasticity*, Clarendon, Oxford, 1968.
33. E. Ramm, 'Strategies for tracing nonlinear responses near limit points', in W. Wunderlich, E. Stein and K. Bathe (eds.), *Nonlinear Finite Element Analysis in Structural Mechanics*, Springer, New York, 1981, pp. 63–89.
34. P. Bergan, G. Horrigamore, B. Krakeland and T. Soreide, 'Solution techniques for nonlinear finite element problems', *Int. J. Numer. Meth. Engng.*, **12**, 1677–1696 (1978).
35. S. W. Lee and T. H. H. Pian, 'Improvement of plate and shell finite elements by mixed formulations', *AIAA J.*, **16**(1), 29–34 (1978).
36. J. C. Simo, D. D. Fox and M. S. Rifai, 'On a stress resultant geometrically exact shell model. Part III: computational aspects of the nonlinear theory', *Comput. Methods Appl. Mech. Engng.*, **79**, 21–70 (1990).
37. D. A. DaDeppo and R. Schmidt, 'Instability of clamped-hinged circular arches subjected to a point load', *J. Appl. Mech.*, **97**, 894–896 (1975).
38. J. Huddleston, 'Finite deflection and snap-through of high circular arches', *J. Appl. Mech.*, **35**, 763–769 (1968).